Title: Targeting BRAF kinase fusions with pan-RAF and vertical MAPK inhibition

Jacqueline A. Turner[1,2], Morgan MacBeth[1], Stacey Bagby[1], Phaedra Whitty[1], Sarah Hartman[1], Dennis Simmons[1], Betelehem Yacob[1], William A. Robinson[1], Kasey L. Couts[1]

[1]Division of Medical Oncology, University of Colorado School of Medicine, Anschutz Medical Campus, Aurora, CO, USA

[2]Medical Scientist Training Program, University of Colorado School of Medicine, Anschutz Medical Campus, Aurora, CO, USA

Corresponding Author: Kasey L. Couts, 12801 E. 17th Ave, MS 8117, Aurora, CO 80045. Kasey.Couts@cuanschutz.edu

Running title: Drug targeting of BRAF kinase fusions

Keywords: kinase, dimerization, pan-RAF inhibitor, paradoxical activation

Conflicts of Interest: The authors of this paper have no conflicts of interest to disclose

Funding: JAT was funded by the Hertz Graduate Fellowship. Additional funding was provided in part by the Amy Davis Foundation, the Moore Family Foundation, and the Heidi Horner Foundation to KLC and WAR.

Abstract

BRAF kinase fusions are a form of structural variation in the genome and are recurrent events in driver-negative melanomas. While *BRAF* fusions reproducibly conserve the kinase domain, there is genetic variability with 5' gene partners and specific *BRAF* breakpoints. We investigated how genetic diversity of *BRAF* kinase fusions affects dimeric signaling and ERK activation. We overexpressed *BRAF* fusions with 5' gene partners including *AGK*, *ZKSCAN1*, *ARMC10*, *PPFIBP2*, and *TRIM24* and found fusion dependent signaling and inhibitor sensitivity. Despite the development of next generation RAF inhibitors, there was paradoxical ERK phosphorylation with multiple pan-RAF inhibitors, which was ameliorated in certain *BRAF* fusions with vertical RAF/MEK inhibition using trametinib and LY3009120. Collectively, we observed some fusion-dependent effects but also tumor growth suppression and resolution of paradoxical activation with vertical pathway inhibition.

Introduction

Activation of the mitogen-activated protein kinase pathway (MAPK) contributes to dysregulated or constitutive signaling in over 85% of all cancers (Bahar et al., 2023; Burotto et al., 2014; Lee et al., 2020; Sinkala et al., 2021). In malignant melanoma, ~50% of all tumors have an activating $BRAF^{V600E}$ mutation and recent studies show there are many other nonclassical mechanisms of pathway activation including kinase fusion, splice variants, and noncanonical mutation (Aya et al., 2024; Davies et al., 2002; Millington, 2013; Nebhan et al., 2021; Turner et al., 2017; Turner et al., 2019). These alternative mechanisms of pathway activation show different responses to MAPK inhibitor therapy (Bahar et al., 2023; Cheng et al., 2013; Nebhan et al., 2021; Turner et al., 2019). *BRAF* gene rearrangement resulting in kinase fusions have genetic heterogeneity with multiple 5' gene partners and 3' *BRAF* breakpoints reported (Botton et al., 2019). The majority of patients are treated with MAPK-directed therapy, specifically MEK inhibition; however, many tumors quickly acquire resistance to these targeted therapies and few reports have demonstrated that some of these targeted therapies result in paradoxical activation (Jung et al., 2021). Thus, targeted therapies, particularly single agent, are generally effective but often not durable clinically (Bahar et al., 2023).

Resistance to MAPK inhibition stems, in part, from BRAF circumventing conserved pathway controls (Bahar et al., 2023; Inamdar et al., 2010; Lee et al., 2020). Typically, BRAF kinases are regulated by conserved regions (CR) including RAS binding domains in CR1 and regulatory phosphorylation of S365 in CR2 (Athuluri-Divakar et al., 2016) (Figure 1a). Yet, V600E mutation within the activation loop of the kinase overcomes these regulatory mechanisms by changing the orientation of the DFG motif, promoting salt bridge formation between the N and C kinase lobes and permitting constitutive monomeric activation (Davies et al., 2002; Mott et al., 1996) (Figure 1b). Protomer transactivation with homo- or heterodimerization with inhibitor bound 'kinase dead' protomers is one mechanism to divert targeted pathway inhibition (Poulikakos

et al., 2010). Heterodimerization with CRAF (the product of *RAF1* gene) is a canonical mechanism of resistance characterized in BRAF or NRAS mutated tumors (Rohrer et al., 2023; Wang et al., 2023). Yet, the relationship between genetic architecture of a fusion construct and sensitivity to MAPK inhibitors beyond MEK inhibition is not well-defined.

BRAF gene fusions have a diverse genetic landscape of 5' gene partners in melanoma which complicates treatment, responses and likely necessitates a more nuanced approach to therapeutic design and patient care. Here, we investigated how variations in *BRAF* fusion kinase genetics could inform drug combination and therapeutic outcomes. Paradoxical activation occurs with multiple RAF inhibitors across *BRAF* fusion constructs, but dual RAF/MEK inhibition with trametinib and LY3009120 improves efficacy over single-agent MEK inhibition and overcomes paradoxical activation in certain *BRAF* fusion models. Here, we propose a more sophisticated rationale for treatment based on mechanistic dimeric BRAF signaling to inform vertical multi-drug pathway inhibition.

Results

BRAF fusions preferentially homo- and heterodimerize

To investigate dimeric BRAF fusion signaling, we transiently overexpressed five different tagged *BRAF* fusions including *AGK-BRAF*, *ZKSCAN1-BRAF*, *ARMC10-BRAF*, *PPFIBP2-BRAF*, and *TRIM24-BRAF* in HEK293T cells (Figure 2a). We preformed co-immunoprecipitation of HA-tagged fusions with either MYC-tagged BRAF fusions, wild type BRAF, or CRAF (Figure 2b). Immunoblotting demonstrates BRAF fusions predominantly homodimerize with fusion protomers or heterodimerization with wild type BRAF. PPFIBP2-BRAF and TRIM24-BRAF primarily homodimerize with their complementary fusion protomer whereas AGK-BRAF, ZKSCAN1-BRAF, and ARMC10-BRAF appeared to engage both reciprocal fusion homodimerization and heterodimerization with wild type BRAF. In certain fusions, there was weak heterodimerization with CRAF best observed in ZKSCAN1-BRAF and ARMC10-BRAF. Altogether, these findings show BRAF fusions cooperate with both wild type BRAF and fusion BRAF dimer partners to signal.

Multiple RAF inhibitors cause paradoxical activation in BRAF fusions

Historically, aberrant BRAF activation has been targeted with vemurafenib, a type I ATP competitive BRAF inhibitor. New "next generation" or "paradox breaking" RAF inhibitors have been developed to address various mechanisms of RAF isoform activation and counteract paradoxical pathway activation (Figure 3a). These inhibitors target DFG-in and αC helix out orientations. One RAF inhibitor, LY3009120, functions as an equipotent pan-RAF inhibitor and uniquely targets αC helix in orientations.

We questioned if BRAF fusions are similarly sensitive to RAF inhibitors and we screened for fusion sensitivity against vemurafenib, MLN2480, PLX8394, and belvarafenib with AGK-BRAF and ZKSCAN1-BRAF expressing cells. We found that paradoxical activation was frequently observed across multiple RAF inhibitors (Figure 3b). Even the paradox breaking BRAF inhibitor, PLX8394, had elevated phospho-ERK at low treatment doses. Yet, LY3009120 treatment effectively resolves paradoxical activation across all the transiently expressed fusions in HEK293T cells. Taken together, these data show paradoxical activation at low doses persists across multiple RAF inhibitors but LY3009120 mitigates paradoxical activation.

RAF/MEK inhibition enhances tumor suppression in BRAF fusion-driven melanomas

In prior work, we have identified *BRAF* gene fusions in human melanoma patient tumors and found significant differences with *in vivo* growth rate and response to MAPK inhibitors across fusions (Turner et al., 2017; Turner et al., 2019). To assess treatment responses in patient-derived cell lines harboring either *AGK-BRAF* fusion (MB 1692 cell line) or *ARMC10-BRAF* fusion (MB 1374 cell line) fusions with pan-RAF or MEK inhibitors. Trametinib effectively suppressed phospho-ERK whereas RAF inhibition induced paradoxical activation (Figure 4a-b). LY3009120 showed minimal paradoxical activation while other RAF inhibitors including MLN2480 and PLX8394 showed hyperactive ERK phosphorylation (Supplemental Figure 1). Patient-derived cell lines treated with belvarafenib were only sensitive at highest concentrations in MB 1692 and was ineffective in MB 1374 (Figure 4c). Whereas single agents trametinib and LY3009120 were more effective at inhibiting phospho-ERK and reducing cell viability.

We then questioned how effective dual inhibition with combination LY3009120 and trametinib would be at blocking ERK phosphorylation. In both patient cell lines, single agent efficacy was enhanced with combination of RAF/MEK inhibition using trametinib and LY3009120 (Figure 5a-b). Combination treatment was also significantly more effective in reducing the specific growth rate (SGR) *in vivo* (Figure 5c-d). While single agent trametinib significantly reduced SGR in MB 1374, it did not achieve a significant effect in the MB 1692 model as previously reported (Turner et al., 2019). Immunoblotting analysis of *in vivo* treated tumors also showed reduction of phosphorylated ERK with combination therapy in both MB 1692 and MB 1374 (Figure 5e-f). Altogether, these data show single agent trametinib and combination therapy with trametinib and LY3009120 are effective at reducing tumor growth, yet the degree of vertical pathway inhibition benefit is fusion dependent.

Discussion

This study demonstrates that BRAF fusions preferentially form specific dimer partners and can exhibit paradoxical activation in response to RAF inhibition. Selective dimerization of BRAF fusions occurs as homodimers with fusion protomers and as heterodimers with wild type BRAF. Paradoxical activation in BRAF fusion constructs occurs with several RAF inhibitors,

necessitating dual inhibition with MEK for improved efficacy in certain tumor models. Our research underscores that single-agent MAPK inhibition may offer limited benefit due to paradoxical activation by RAF inhibitors, whereas combination therapy with trametinib and LY3009120 could be more effective.

We observed preferential dimerization of BRAF fusions and infrequent coordination with CRAF protomers. Importantly, we transiently overexpressed these fusion constructs in HEK293T cells, ensuring no prior treatment or other activating background alterations that could impact dimer selectivity. Given that CRAF signaling is a frequent mechanism of MAPK inhibitor escape via BRAF-CRAF heterodimerization (Murphy et al., 2022; Weber et al., 2001), we cannot exclude that CRAF heterodimerization could act as a resistance mechanism for fusion-driven pathways. While *BRAF* fusion is a known mechanism of RAS-independent MAPK signaling (Haling et al., 2014; Yao et al., 2019), it could be possible that RAS isotypes are still able to cooperate with BRAF fusion protomers and promote asymmetric transactivation. Regardless, LY3009120 equipotently targets pan-RAF protomers (Peng et al., 2015) and may be effectively blocking heterodimeric asymmetric transactivation.

Active RAF dimers transmit signals downstream to ERK which has numerous phosphorylation targets both in the cytoplasm and in the nucleus (Gardner et al., 1994; Graves et al., 1995; Haling et al., 2014; Lavoie et al., 2020; Lee et al., 2020; Liu et al., 2018). Our prior research showed that patient-derived xenografts harboring *AGK-BRAF*, *ARMC10-BRAF*, or *SEPT3-BRAF* fusions demonstrated varied ERK subcellular localization when treated with MAPK inhibitors (Turner et al., 2019). Particularly, the *ARMC10-BRAF* fusion showed prominent nuclear ERK localization in both untreated and vemurafenib-resistant tumors, whereas other fusion constructs and MAPK inhibitor-sensitive tumors did not (Turner et al., 2019). ERK localization could regulate feedback on MAPK signaling and play a contributory role in paradoxical pathway activation.

In this study, we even observed paradox-breaking RAF inhibitors fail to block activation in BRAF fusions while LY3009120 mitigated paradox activation in MB 1692. Interestingly, LY3009120 is the only RAF inhibitor that we tested which targets αC helix in orientations (Peng et al., 2015). Previous studies postulate that selective binding of BRAF inhibitors alleviates an inhibitory phosphorylation of the P loop on RAF1 (Holderfield et al., 2014; Kohler et al., 2016). Interestingly, LY3009120 induces BRAF-CRAF heterodimerization but equipotently inhibits MEK/ERK activation regardless of dimer pairs (Adamopoulos et al., 2021; Peng et al., 2015). We observed minimal paradoxical activation with single agent LY3009120 and in certain fusion backgrounds there was improved growth inhibition and pathway suppression with multidrug targeting. Yet, there are still fusion-dependent effects, and we likely may be able to exploit dual RAF/MEK inhibition to counteract paradoxical activation.

Based on our findings presented here, we propose to use genetic and molecular features to help inform drug targeting. As demonstrated, there may be certain patient BRAF fusions that have

varying degrees of benefit and be more sensitive to single agent trametinib versus combination therapy with RAF/MEK inhibition. Genetic architecture and molecular behavior including *BRAF* breakpoints, 5' gene partners, and dimeric signaling could affect patient responses and treatment should be tailored to the genetic and molecular heterogeneity of the *BRAF* gene fusion.

Methods

Plasmids and gene constructs

AGK-BRAF, *ZKSCAN1-BRAF*, *ARMC10-BRAF*, *PPFIBP2-BRAF*, and *TRIM24-BRAF* cDNA sequences were generated by GenScript Biotech (Piscataway, NJ, USA). HA and MYC tagged cDNA sequences were also generated by GenScript for *BRAF* fusion-HA tag, free MYC tag, *BRAF* fusion-MYC tag, wild type *BRAF*-MYC tag, or wild type *RAF1*-MYC tag. Sequences were cloned into the pLVX-EF1α-IRES-ZsGreen1 vector (Clonetech Laboratories Inc., Fremont, CA, USA) using the One Shot® Mach1™ T1 Phage-Resistant Chemically Competent *E. coli* (Invitrogen). Midi Prep DNAs were generated using the HiSpeed® Plasmid Midi Kit (Qiagen).

Transient gene expression and treatment

HEK293T cells were first seeded with 750,000 cells per 6 cm tissue culture dishes. Cells were transiently transfected with gene constructs and plasmids as detailed above. Twenty-four hours later, cells were transfected with Lipofectamine LTX & PLUS (Invitrogen) with 0.915 µg DNA. Cells were incubated at 37°C for 48 hours. Cells were then serum starved for 6 hours and treated with varying concentration of drugs as follows: Vemurafenib (0, 1, 10, 100, or 1000nM), MLN2480 (0, 1, 10, 100, or 1000nM), PLX8394 (0, 5, 50, 500, 5000nM), belvarafenib (0, 0.1, 1, 10, 100nM), LY3009120 (0, 5, 50, 500, 5000nM), and trametinib (0, 0.1, 1, 10, 100nM). HEK293T cells were STR profiled and mycoplasma tested.

In vivo treatment studies

As previously described, patient-derived xenografts were generated from melanoma tumor samples collected at the University of Colorado Hospital (Turner et al., 2019; Turner et al., 2024). Melanoma tumor samples were collected with patient consent and approval from the Colorado Multiple Institutional Review Board (#05-0309) at the University of Colorado Cancer Center. Patient studies were conducted according to the Declaration of Helsinki, the Belmont Report, and the U.S. Common Rule. All animal work and care were performed under the guidelines of the University of Colorado Anschutz Medical Campus Institutional Animal Care and Use Committee (IACUC).

For treatment studies, tumors were implanted subcutaneously bilaterally into approximately 10-week-old nude, female mice (Inotiv, Hsd:Athymic Nude-Foxn1nu). Mice were randomized when tumors reached an average of ~100-300 mm^3 into three groups per model including vehicle, trametinib (dosed 100 µl at 1 mg/kg orally once daily, 0.5 mg/kg for

combination studies, vehicle made in 5 mL 10% Cremophor EL, 5 mL 10% polyethylene glycol, and 40 mL water and sonicated for 1 hour prior to use), LY3009120 (dosed 100 µl at 30 mg/kg orally twice daily, vehicle made in 4% DMSO, 30% polyethylene glycol 400, %% Tween80 with sonication for 5 minutes after adding DMSO and then sonicate for 1 hour after adding vehicle reagents). Each group had 7-8 mice per group with one tumor per flank (with 1-2 tumors injected per mouse). Drug compounds were purchased from LC Laboratories. Tumor volume was measured at least twice per week using digital calipers and Study Director software package (Studylog Systems) and determined based on the following equation, Tumor Volume = [length x width^2] x 0.52. Specific growth grate (SGR) was determined after the end of study using the following equation, SGR = $\ln(V_2/V_1)/(T_2-T_1)$ where V_1 represents the first volume measurement (that is not zero) in mm^3, V_2 represents the final volume measurement in mm^3, T_1 represents the first day of measurement (that is not zero), T_2 represents the final day of measurement. Throughout tumor studies, individual mouse weights were measured twice weekly and mice were observed for any treatment side effects.

Melanoma cell lines and i*n vitro* treatment studies

As previously described, patient-derived cell lines MB 1692 and MB 1374 were generated from melanoma tumor samples collected at the University of Colorado Hospital (Turner et al., 2019; Turner et al., 2024). Cells were maintained in RPMI supplemented with 10% FBS and 1% penicillin-streptomycin in 37°C incubators with 5% CO_2. All cell lines were profiled using STR DNA Profiling Globalfiler (Thermo Fisher Scientific) and mycoplasma tested. Patient-derived cell lines were plated with 750,000 cells per 6 cm tissue culture dishes and 48 hours later were serum starved for 6 hours and treated with varying concentrations of drugs as follows: Vemurafenib (0, 1, 10, 100, or 1000nM), MLN2480 (0, 1, 10, 100, or 1000nM), PLX8394 (0, 5, 50, 500, 5000nM), belvarafenib (0, 0.1, 1, 10, 100nM), LY3009120 (0, 5, 50, 500, 5000nM), and trametinib (0, 0.1, 1, 10, 100nM). Combination treatments were also done with the following doses: Trametinib 1 or 5nm and LY3009120 500 and 5000nM.

Cell Viability

Patient cell lines were plated between 2000 and 4000 cells per well in black, flat, clear bottomed 96-well plates and treated with inhibitors in triplicate. Inhibitor compounds were purchased from SelleckChem. Cells were then treated with inhibitors 24 hours after plating at 37°C. After 72 hours, cell viability was determined after using the luminescence Cell Titer Glo assay (Promega) on the BioTek Synergy HTX plate reader. Data was graphed and analyzed in graphpad.

Western immunoblotting

Cells were plated, treated, and prepared as described above. Tumors were harvested from mice as described above. Samples were lysed using complete RIPA buffer (RIPA + protease inhibitor + phosphatase inhibitor, Thermo Fisher Scientific) for 10 minutes. The Qiagen

TissueLyser II was used to mechanically homogenize tumor samples. Lysate supernatants were collected after centrifugation at 13,000 rpm for 10 minutes. Fifty µg of protein was loaded into an SDS-PAGE and transferred onto nitrocellulose membranes using iBlot 2 Transfer (Thermo Fisher Scientific). Protein was visualized on blot membranes using the following primary antibodies from Cell Signaling Technology (Danvers, MA, USA): phospho-BRAF (Ser445, #2696), phospho-MEK1/2 (Ser217/221, #9121), MEK1/2 (#9122), phospho-ERK1/2 (Thr202/Tyr204, #4370), and ERK1/2 (#9102), β-actin (#4970). Blot membranes were incubated with fluorescent secondary mouse and rabbit antibodies from Li-Cor (Lincoln, NE, USA). Protein was visualized on the Li-Cor Odyssey and protein was quantified using Fiji software.

Co-immunoprecipitation

Individually tagged HA-tagged BRAF fusions were co-immunoprecipitated with their potential dimerization partners. Total protein from lysates were collected (as described above). HA-tagged proteins were immunoprecipitated by using a magnetic bead immunoprecipitation (IP) pull down columns. HA-tagged proteins were bound with bead conjugated anti-HA antibody run through a magnetic chromatography column. Bound protein was then eluted, washed, and collected for immunoblotting. Protein was visualized on immunoblots with anti-HA antibody (top blots in Figure 2B) or anti-MYC antibody (bottom blots in Figure 2B).

References

Adamopoulos, C., T.A. Ahmed, M.R. Tucker, P.M.U. Ung, M. Xiao, Z. Karoulia, A. Amabile, X. Wu, S.A. Aaronson, C. Ang, V.W. Rebecca, B.D. Brown, A. Schlessinger, M. Herlyn, Q. Wang, D.E. Shaw, and P.I. Poulikakos. 2021. Exploiting Allosteric Properties of RAF and MEK Inhibitors to Target Therapy-Resistant Tumors Driven by Oncogenic BRAF Signaling. *Cancer Discov*. 11:1716-1735.

Athuluri-Divakar, S.K., R. Vasquez-Del Carpio, K. Dutta, S.J. Baker, S.C. Cosenza, I. Basu, Y.K. Gupta, M.V. Reddy, L. Ueno, J.R. Hart, P.K. Vogt, D. Mulholland, C. Guha, A.K. Aggarwal, and E.P. Reddy. 2016. A Small Molecule RAS-Mimetic Disrupts RAS Association with Effector Proteins to Block Signaling. *Cell*. 165:643-655.

Aya, F., P. Lanuza-Gracia, A. Gonzalez-Perez, S. Bonnal, E. Mancini, N. Lopez-Bigas, A. Arance, and J. Valcarcel. 2024. Genomic deletions explain the generation of alternative BRAF isoforms conferring resistance to MAPK inhibitors in melanoma. *Cell Rep*. 43:114048.

Bahar, M.E., H.J. Kim, and D.R. Kim. 2023. Targeting the RAS/RAF/MAPK pathway for cancer therapy: from mechanism to clinical studies. *Signal Transduct Target Ther*. 8:455.

Botton, T., E. Talevich, V.K. Mishra, T. Zhang, A.H. Shain, C. Berquet, A. Gagnon, R.L. Judson, R. Ballotti, A. Ribas, M. Herlyn, S. Rocchi, K.M. Brown, N.K. Hayward, I. Yeh, and B.C. Bastian. 2019. Genetic Heterogeneity of BRAF Fusion Kinases in Melanoma Affects Drug Responses. *Cell Rep*. 29:573-588 e577.

Burotto, M., V.L. Chiou, J.M. Lee, and E.C. Kohn. 2014. The MAPK pathway across different malignancies: a new perspective. *Cancer*. 120:3446-3456.

Cheng, Y., G. Zhang, and G. Li. 2013. Targeting MAPK pathway in melanoma therapy. *Cancer Metastasis Rev*. 32:567-584.

Davies, H., G.R. Bignell, C. Cox, P. Stephens, S. Edkins, S. Clegg, J. Teague, H. Woffendin, M.J. Garnett, W. Bottomley, N. Davis, E. Dicks, R. Ewing, Y. Floyd, K. Gray, S. Hall, R. Hawes, J. Hughes, V. Kosmidou, A. Menzies, C. Mould, A. Parker, C. Stevens, S. Watt, S. Hooper, R. Wilson, H. Jayatilake, B.A. Gusterson, C. Cooper, J. Shipley, D. Hargrave, K. Pritchard-Jones, N. Maitland, G. Chenevix-Trench, G.J. Riggins, D.D. Bigner, G. Palmieri, A. Cossu, A. Flanagan, A. Nicholson, J.W. Ho, S.Y. Leung, S.T. Yuen, B.L. Weber, H.F. Seigler, T.L. Darrow, H. Paterson, R. Marais, C.J. Marshall, R. Wooster, M.R. Stratton, and P.A. Futreal. 2002. Mutations of the BRAF gene in human cancer. *Nature*. 417:949-954.

Gardner, A.M., R.R. Vaillancourt, C.A. Lange-Carter, and G.L. Johnson. 1994. MEK-1 phosphorylation by MEK kinase, Raf, and mitogen-activated protein kinase: analysis of phosphopeptides and regulation of activity. *Mol Biol Cell*. 5:193-201.

Graves, J.D., J.S. Campbell, and E.G. Krebs. 1995. Protein serine/threonine kinases of the MAPK cascade. *Ann N Y Acad Sci*. 766:320-343.

Haling, J.R., J. Sudhamsu, I. Yen, S. Sideris, W. Sandoval, W. Phung, B.J. Bravo, A.M. Giannetti, A. Peck, A. Masselot, T. Morales, D. Smith, B.J. Brandhuber, S.G. Hymowitz, and S. Malek. 2014. Structure of the BRAF-MEK complex reveals a kinase activity independent role for BRAF in MAPK signaling. *Cancer Cell*. 26:402-413.

Holderfield, M., M.M. Deuker, F. McCormick, and M. McMahon. 2014. Targeting RAF kinases for cancer therapy: BRAF-mutated melanoma and beyond. *Nat Rev Cancer*. 14:455-467.

Inamdar, G.S., S.V. Madhunapantula, and G.P. Robertson. 2010. Targeting the MAPK pathway in melanoma: why some approaches succeed and other fail. *Biochem Pharmacol*. 80:624-637.

Jung, T., M. Haist, M. Kuske, S. Grabbe, and M. Bros. 2021. Immunomodulatory Properties of BRAF and MEK Inhibitors Used for Melanoma Therapy-Paradoxical ERK Activation and Beyond. *Int J Mol Sci*. 22.

Kohler, M., M. Roring, B. Schorch, K. Heilmann, N. Stickel, G.J. Fiala, L.C. Schmitt, S. Braun, S. Ehrenfeld, F.M. Uhl, T. Kaltenbacher, F. Weinberg, S. Herzog, R. Zeiser, W.W. Schamel, H. Jumaa, and T. Brummer. 2016. Activation loop phosphorylation regulates B-Raf in vivo and transformation by B-Raf mutants. *EMBO J*. 35:143-161.

Lavoie, H., J. Gagnon, and M. Therrien. 2020. ERK signalling: a master regulator of cell behaviour, life and fate. *Nat Rev Mol Cell Biol*. 21:607-632.

Lee, S., J. Rauch, and W. Kolch. 2020. Targeting MAPK Signaling in Cancer: Mechanisms of Drug Resistance and Sensitivity. *Int J Mol Sci*. 21.

Liu, F., X. Yang, M. Geng, and M. Huang. 2018. Targeting ERK, an Achilles' Heel of the MAPK pathway, in cancer therapy. *Acta Pharm Sin B*. 8:552-562.

Millington, G.W. 2013. Mutations of the BRAF gene in human cancer, by Davies et al. (Nature 2002; 417: 949-54). *Clin Exp Dermatol*. 38:222-223.

Mott, H.R., J.W. Carpenter, S. Zhong, S. Ghosh, R.M. Bell, and S.L. Campbell. 1996. The solution structure of the Raf-1 cysteine-rich domain: a novel ras and phospholipid binding site. *Proc Natl Acad Sci U S A*. 93:8312-8317.

Murphy, B.M., E.M. Terrell, V.R. Chirasani, T.J. Weiss, R.E. Lew, A.M. Holderbaum, A. Dhakal, V. Posada, M. Fort, M.S. Bodnar, L.M. Carey, M. Chen, C.J. Burd, V. Coppola, D.K. Morrison, S.L. Campbell, and C.E. Burd. 2022. Enhanced BRAF engagement by NRAS mutants capable of promoting melanoma initiation. *Nat Commun*. 13:3153.

Nebhan, C.A., D.B. Johnson, R.J. Sullivan, R.N. Amaria, K.T. Flaherty, J.A. Sosman, and M.A. Davies. 2021. Efficacy and Safety of Trametinib in Non-V600 BRAF Mutant Melanoma: A Phase II Study. *Oncologist*. 26:731-e1498.

Peng, S.B., J.R. Henry, M.D. Kaufman, W.P. Lu, B.D. Smith, S. Vogeti, T.J. Rutkoski, S. Wise, L. Chun, Y. Zhang, R.D. Van Horn, T. Yin, X. Zhang, V. Yadav, S.H. Chen, X. Gong, X. Ma, Y. Webster, S. Buchanan, I. Mochalkin, L. Huber, L. Kays, G.P. Donoho, J. Walgren, D. McCann, P. Patel, I. Conti, G.D. Plowman, J.J. Starling, and D.L. Flynn. 2015. Inhibition of RAF Isoforms and Active Dimers by LY3009120 Leads to Anti-tumor Activities in RAS or BRAF Mutant Cancers. *Cancer Cell*. 28:384-398.

Poulikakos, P.I., C. Zhang, G. Bollag, K.M. Shokat, and N. Rosen. 2010. RAF inhibitors transactivate RAF dimers and ERK signalling in cells with wild-type BRAF. *Nature*. 464:427-430.

Rohrer, L., C. Spohr, C. Beha, R. Griffin, S. Braun, S. Halbach, and T. Brummer. 2023. Analysis of RAS and drug induced homo- and heterodimerization of RAF and KSR1 proteins in living cells using split Nanoluc luciferase. *Cell Commun Signal*. 21:136.

Sinkala, M., P. Nkhoma, N. Mulder, and D.P. Martin. 2021. Integrated molecular characterisation of the MAPK pathways in human cancers reveals pharmacologically vulnerable mutations and gene dependencies. *Commun Biol*. 4:9.

Turner, J., K. Couts, J. Sheren, S. Saichaemchan, W. Ariyawutyakorn, I. Avolio, E. Cabral, M. Glogowska, C. Amato, S. Robinson, J. Hintzsche, A. Applegate, E. Seelenfreund, R. Gonzalez, K. Wells, S. Bagby, J. Tentler, A.C. Tan, J. Wisell, M. Varella-Garcia, and W. Robinson. 2017. Kinase gene fusions in defined subsets of melanoma. *Pigment Cell Melanoma Res*. 30:53-62.

Turner, J.A., J.G.T. Bemis, S.M. Bagby, A. Capasso, B.W. Yacob, T.S. Chimed, R. Van Gulick, H. Lee, R. Tobin, J.J. Tentler, T. Pitts, M. McCarter, W.A. Robinson, and K.L. Couts. 2019. BRAF fusions identified in melanomas have variable treatment responses and phenotypes. *Oncogene*. 38:1296-1308.

Turner, J.A., R.J. Van Gulick, W.A. Robinson, T. Mughal, R.P. Tobin, M.L. MacBeth, B. Holman, A. Classon, S.M. Bagby, B.W. Yacob, S.J. Hartman, I. Silverman, V.M. Vorwald, N. Gorden, R. Gonzalez, L.M. Gay, S.M. Ali, A. Benson, V.A. Miller, J.S. Ross, T.M. Pitts, M.J. Rioth, K.D. Lewis, T. Medina, M.D. McCarter, R. Gonzalez, and K.L. Couts. 2024. Expanding the landscape of oncogenic drivers and treatment options in acral and mucosal melanomas by targeted genomic profiling. *Int J Cancer*.

Wang, P., K. Laster, X. Jia, Z. Dong, and K. Liu. 2023. Targeting CRAF kinase in anti-cancer therapy: progress and opportunities. *Mol Cancer*. 22:208.

Weber, C.K., J.R. Slupsky, H.A. Kalmes, and U.R. Rapp. 2001. Active Ras induces heterodimerization of cRaf and BRaf. *Cancer Res*. 61:3595-3598.

Yao, Z., Y. Gao, W. Su, R. Yaeger, J. Tao, N. Na, Y. Zhang, C. Zhang, A. Rymar, A. Tao, N.M. Timaul, R. McGriskin, N.A. Outmezguine, H. Zhao, Q. Chang, B. Qeriqi, M. Barbacid, E. de Stanchina, D.M. Hyman, G. Bollag, and N. Rosen. 2019. RAF inhibitor PLX8394 selectively disrupts BRAF dimers and RAS-independent BRAF-mutant-driven signaling. *Nat Med*. 25:284-291.

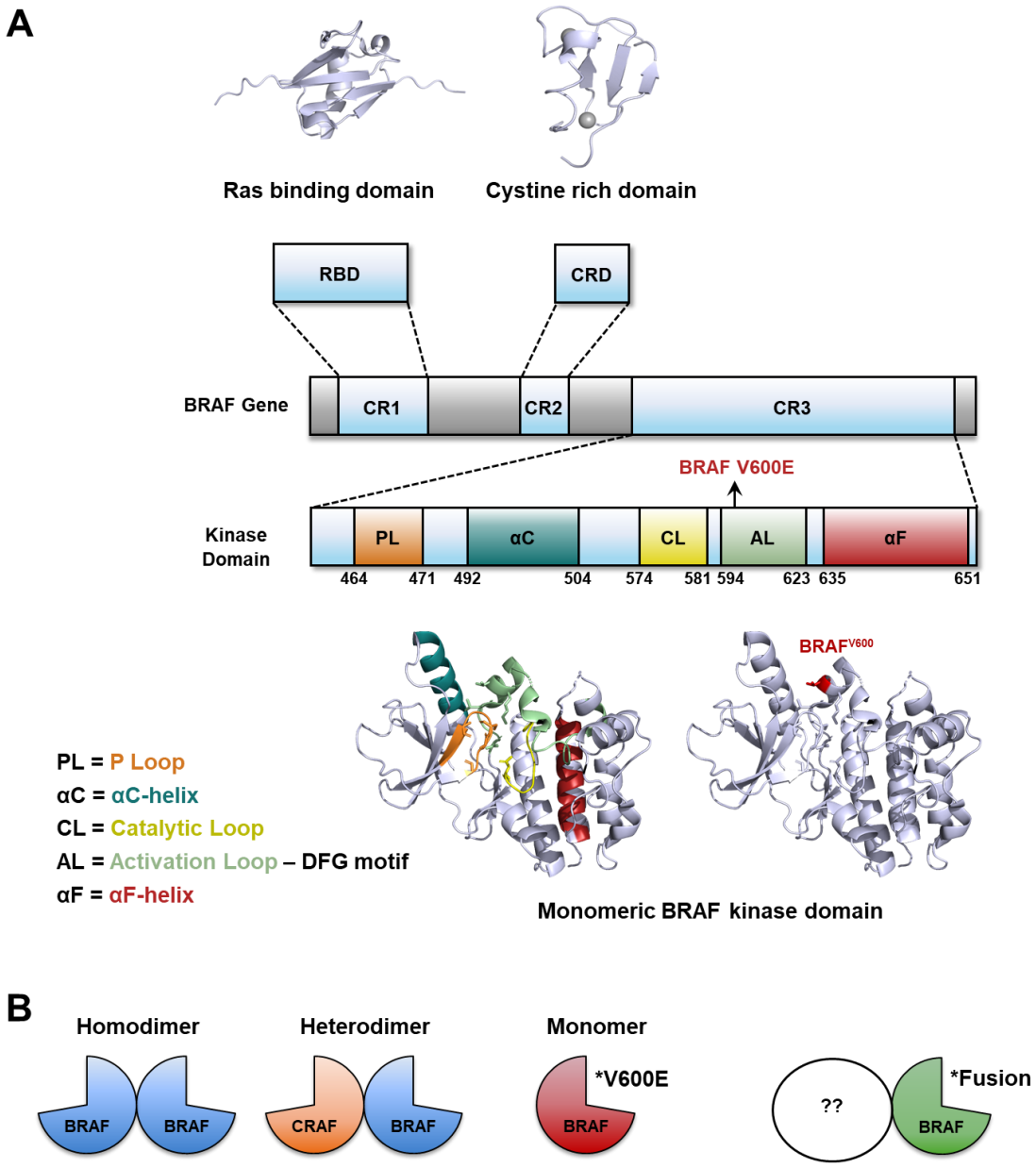

Figure 1. Crystal structure and schematic representation of BRAF domains, fusion constructs, and dimer signaling. (A) Crystal structures from domains within the BRAF gene including the RAS binding domain (RBD, PDB ID: 5J17), cystine rich domain (CRD, PDB ID: 1FAQ), and the monomeric BRAF kinase fusion (PDB ID: 4WO5). Within the BRAF kinase, loops and helices are highlighted by the following colors: orange designates the P Loop, dark green designates the αC-helix, yellow designates the catalytic loop, green designates the activation loop, and red designates the αF-helix. **(B)** Schematic of RAF protomer signaling and dimerization. Blue designates BRAF protomers homodimerizing or heterodimerizing. Orange designates RAF1 (or CRAF) protomer heterodimerizing. Red designates the valine residue $BRAF^{V600}$ on the protomer. Green indicates fusion BRAF protomers with unknown signaling partners.

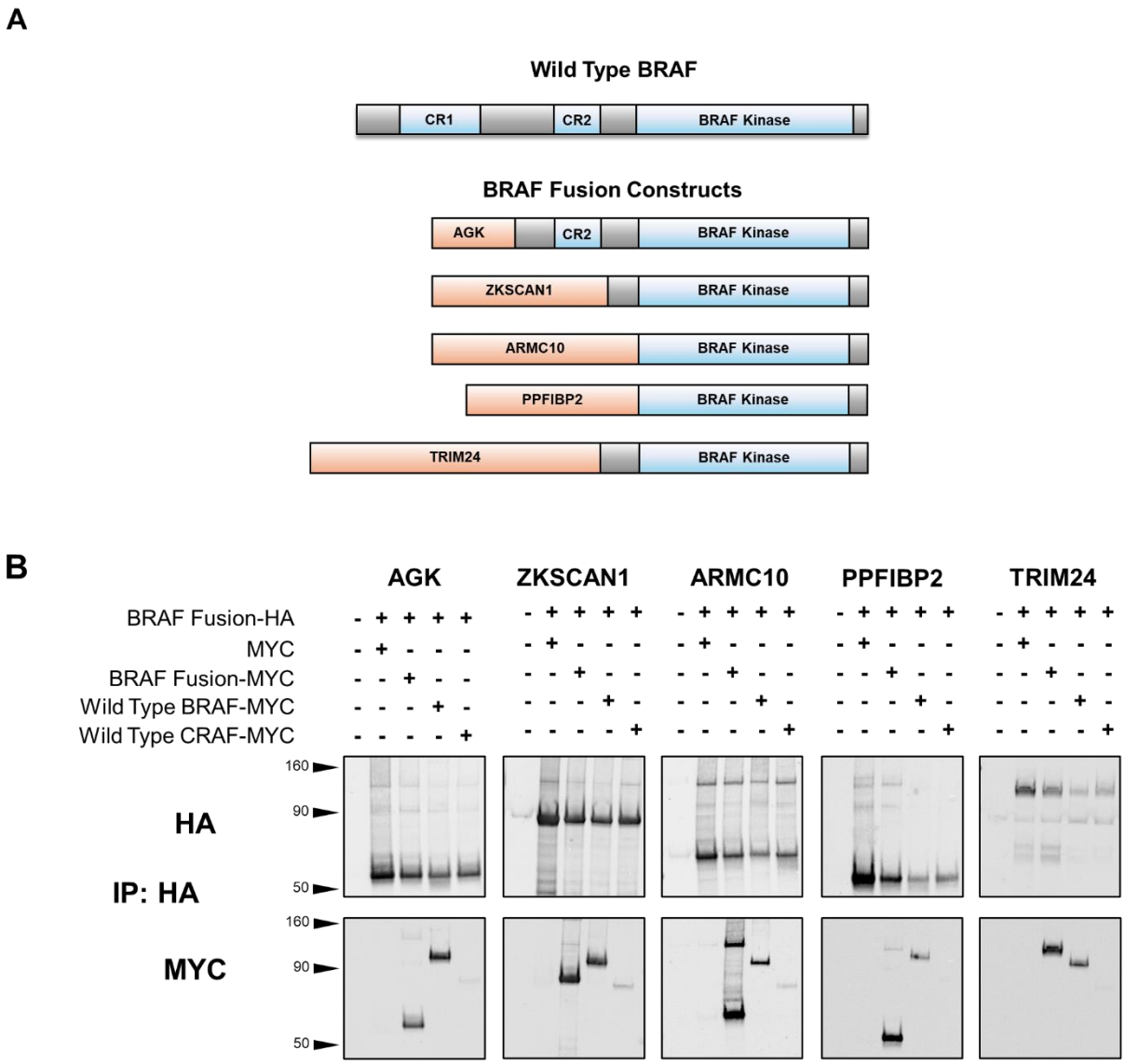

Figure 2. BRAF kinase fusions activate the MAPK pathway through fusion homodimerization and heterodimerization with wild type BRAF. (A) Genetic constructs of wild type *BRAF* and *BRAF* fusion constructs. Conserved region 1 is highlighted in wild type *BRAF* as CR1. Conserved region 2 is highlighted in wild type *BRAF* and *AGK-BRAF* as CR2. **(B)** Dimerization partners are determined by co-immunoprecipitation of HA-tagged proteins and then blotted for either the pulled down HA-tagged fusion protein (BRAF Fusion-HA) or co-transfected MYC-tagged constructs including free MYC (unbound by HA tagged BRAF fusions), BRAF Fusion-MYC, Wild Type BRAF-MYC, and Wild Type RAF1-MYC.

A

Compound	Target	DFG Conformation	αC Helix Orientation
Vemurafenib	ATP Competitive BRAF	In	Out
MLN2480 (TAK-580)	ATP Competitive Pan-RAF	In	Out
PLX8394	Paradox Breaker BRAF	In	Out
Belvarafenib	Dimer Selective BRAF	In	Out
LY3009120	Equipotent Pan-RAF	In	In

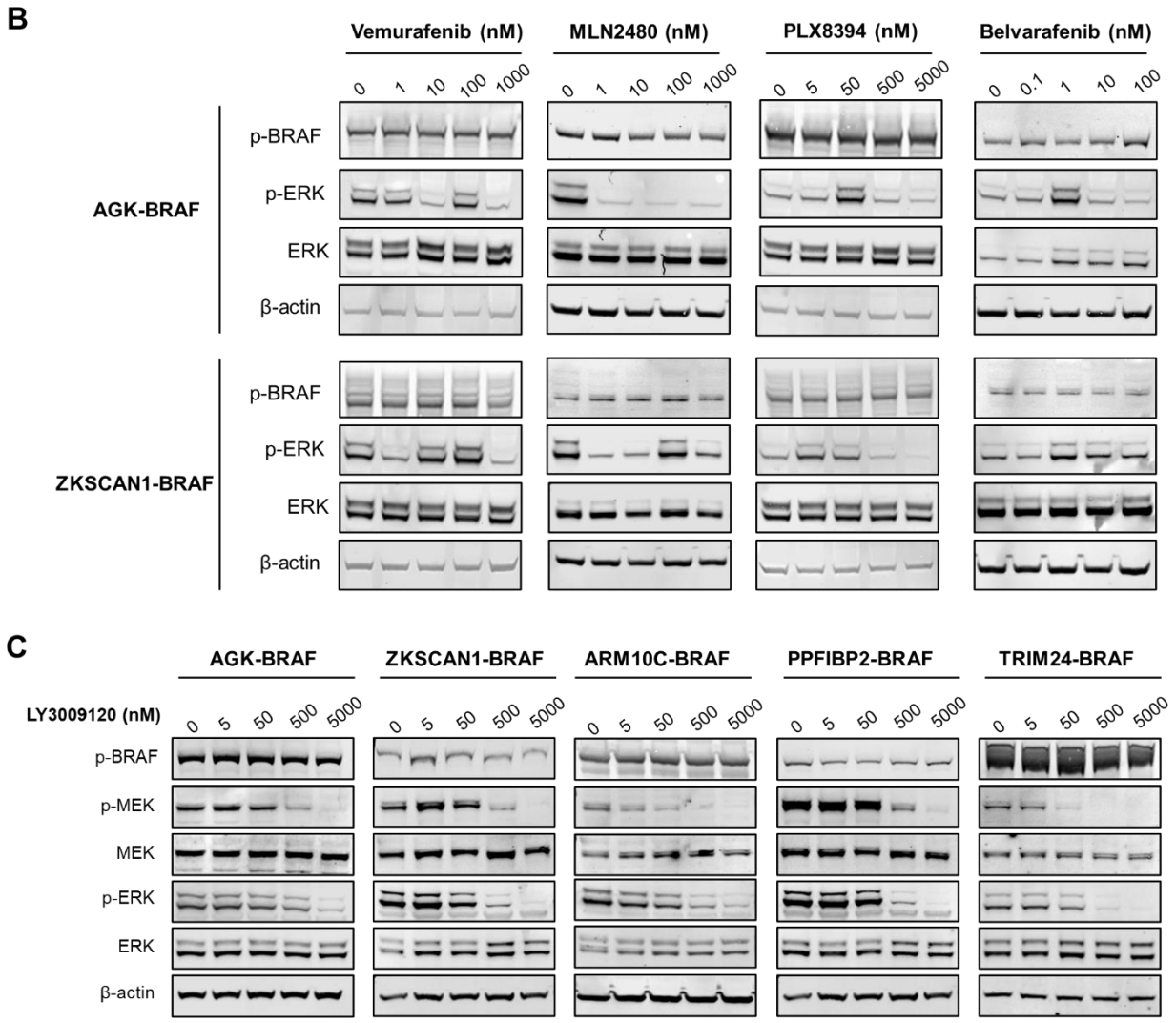

Figure 3. Screening RAF inhibitors shows most RAF inhibitors cause paradoxical activation at low doses whereas LY3009120 overcomes paradoxical activation across fusion constructs. **(A)** RAF kinase inhibitors and compound characteristics. **(B)** MAPK immunoblotting on treatment of transiently overexpressed kinase fusions *AGK-BRAF* and *ZKSCAN1-BRAF* with RAF inhibitor compounds, vemurafenib, MLN2480, PLX8394, and belvarafenib. **(C)** Treatment of transiently overexpressed kinase fusions *AGK-BRAF*, *ZKSCAN1-BRAF*, *ARMC10-BRAF*, *PPFIBP2-BRAF*, *TRIM24-BRAF* with pan-RAF inhibitor, LY3009120.

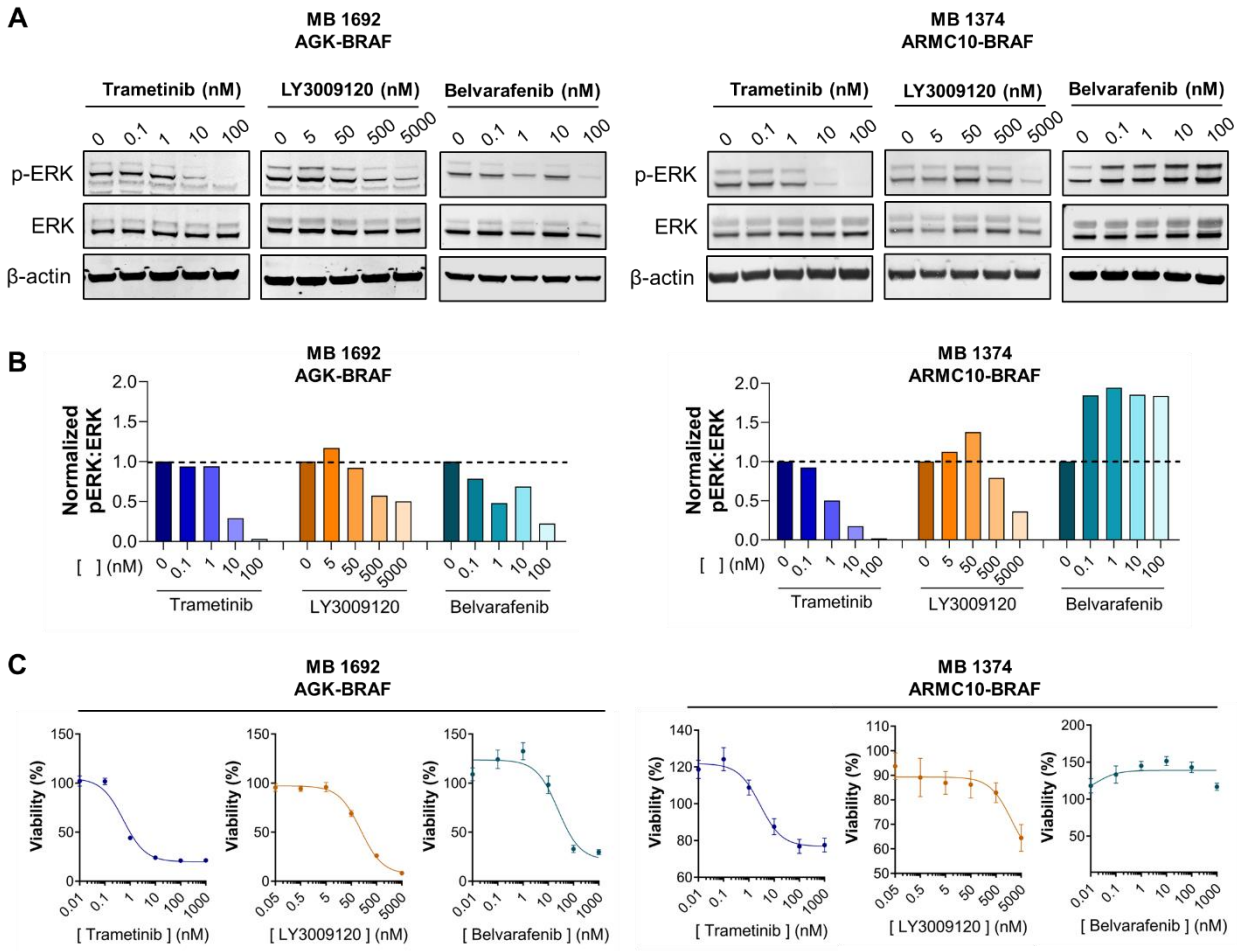

Figure 4. Targeting endogenous BRAF kinase fusions in patient-derived cell lines with MAPK inhibitors. (A) ERK immunoblotting in patient derived cell lines MB 1692 and MB 1374 harboring *AGK-BRAF* and *ARMC10-BRAF* fusions respectively. Fusion cell lines were treated with trametinib, LY3009120, or belvarafenib. **(B)** Quantification of western immunoblots represented in in panel (A) with bars representing normalized amounts of phosphorylated ERK to total ERK. **(C)** Patient-derived cell viability of BRAF fusions treated with MEK/RAF inhibitors, trametinib, LY3009120, or belvarafenib. Error bars represent standard error of the mean of technical triplicates.

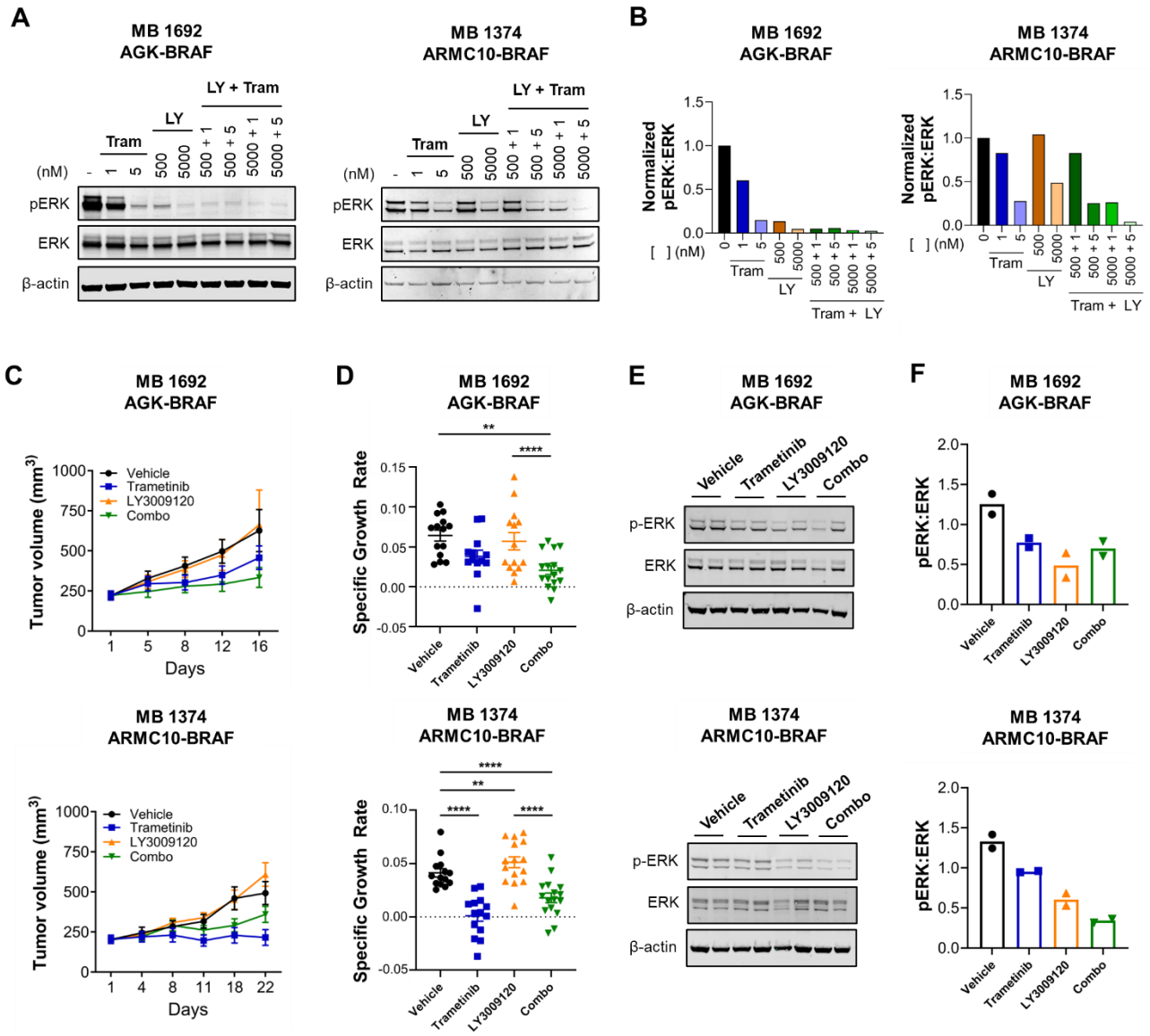

Figure 5. Benefit for vertical pathway inhibition with trametinib and LY3009120 is fusion dependent. (A) ERK immunoblotting of MAPK inhibitor treatment with trametinib (Tram), LY3009120 (LY), combination (LY + Tram). **(B)** Quantification of western immunoblots represented in in panel (A) with bars representing normalized amounts of phosphorylated ERK to total ERK. **(C)** Patient-derived xenograft (PDX) tumor models of MB 1692 or MB 1374 harboring *AGK-BRAF* and *ARMC10-BRAF* fusions respectively and treated with MAPK inhibitors, vehicle, trametinib (1 mg/kg orally once daily), LY3009120 (30 mg/kg orally twice daily). Tumor volume is shown, and error bars represent the standard error of the mean (n = 7-8 mice per group each with one tumor per flank). **(D)** Calculated specific growth rates per tumor based on tumor study from panel (C). Statistics were performed using an ANOVA statistical test with Tukey's post-hoc analysis was performed where *$p < 0.05$, **$p < 0.005$, ***$p < 0.0005$, and ****$p < 0.0001$. Error bars represent standard error of the mean. **(E)** ERK immunoblotting from PDX tumors collected at the end of study from panel (C). Data represents two tumors per treatment group per model. **(F)** Quantification of western immunoblots represented in in panel (E) with bars representing normalized amounts of phosphorylated ERK to total ERK.